Synthesis and Characterization of Mixed TiO_2/ZrO_2 Glass Composite Membranes

T. Uma* and M. Nogami*

Department of Materials Science and Engineering, Nagoya Institute of Technology, Showa, Nagoya, 466-8555, Japan

Received: June 27, 2007; In Final Form: August 10, 2007

Phosphosilicate glass membranes doped with a mixture of titania oxide (TiO_2) and zirconium oxide (ZrO_2) were prepared. Fourier transform infrared (FTIR) spectroscopy, thermal gravimetric and differential thermal analysis, pore, impedance, and permeability studies as well as electrochemical analysis were carried out. The specific surface area and pore distributions were described by the Brunauer−Emmett−Teller (BET) method, and the average pore size was found to be approximately 2.2 nm for all composite glass membranes. The FTIR analysis displayed a maximum intensity in the range of 1000−1200 cm^{-1}, indicating the presence of Si−O−Si bonds in the glass composites. A high proton conductivity of 5.8×10^{-3} S cm^{-1} was obtained for one of the membranes at 80 °C and 50% RH. The permeability was measured for a hydrogen flow background and was found to decrease from 1.41×10^{-11} to 3.83×10^{-12} mol/cm s Pa as the temperature from 30 to 110 °C.

1. Introduction

A high proton conducting solid can, in principle, be applied to many devices for hydrogen and hydrogen-containing compounds in the fields of sensors, energy conversion, synthesis of chemicals, and separation of hydrogen.[1,2] These devices are based on an electrochemical cell in which the proton conducting solid is used as an electrolyte. The cell involves electrochemical reactions at each electrode (cathode and anode), and in general, these reactions are desired to be smooth for the devices. Proton conductive solids are also favorable materials as solid electrolytes for such fuel cells. Titania/silica materials are of great importance as glasses especially in advanced material applications,[3,4] catalysts,[5] and selective oxidation reactions.[6,7] The resulting porosity and homogeneity at the atomic level of titania/silica mixed oxides have been associated with differences in their preparation.[8] Schattka et al. synthesized porous TiO_2−ZrO_2− mixtures by polymer gel templating and obtained higher catalytic activities than in the component. However, this method resulted in pore sizes in the micrometer scale.[9] Glass/ceramic materials are solid materials with a crystalline structure obtained by the controlled diversification of the glasses. To fabricate a glass/ceramic product, the glass is melted, formed into the desired shape, and heat-treated to allow the molecules in the glass to connect and order themselves into a crystalline structure. The influence of the preparation method of Ti/Si mixed oxides[10,11] and Zr/Si mixed oxides[12,13] on the resulting material properties has been reviewed.

Low-temperature fuel cells, in particular proton exchange membrane (PEM) fuel cells, are the most suited for transport applications since there are no problems with temperature cycling. The technology of fuel cells working at temperatures lower than 100 °C and using hydrogen as fuel is presently well-established.[14−16] For efficient fuel cells, the protonic conductor separating the electrodes must preferably be prepared as very thin, albeit hydrogen-impermeable, glass membranes. Furthermore, they must be very resistant to the oxidation and possess conductivities $\geq 10^{-2}$ S cm^{-1}.

Recently, our research group has reported on[17,18] the synthesis and preparation of TiO_2 and ZrO_2 mixed with phosphosilicate gels and the investigation of these electrolytes in H_2/O_2 fuel cell tests. To achieve these targets, TiO_2/ZrO_2−P_2O_5−SiO_2 nanocomposite glass membranes were first characterized by experimental techniques including N_2 adsoption−desorption, thermal gravimetric and differential thermal analysis (TG/DTA), impedance spectroscopy, hydrogen permeability measurements, and Fourier transform infrared spectroscopy (FTIR). Ultimately, the sol−gel-derived glass composite membrane was investigated in fuel cell tests at room temperature, and the system exhibited a very good and stable performance at this temperature. In the present, a new class of proton conducting glass composite membranes (GCM) is being designed and developed. Such membranes are expected to possess proton conductivities exceeding 10^{-3} S cm^{-1} at room temperature and superior thermal, mechanical, chemical, and electrochemical stabilities. The mixed inorganic TiO_2/ZrO_2−P_2O_5−SiO_2 glass composite membranes are a suitable candidate for low-temperature H_2/O_2 fuel cell applications.

2. Experimental Procedures

2.1. Materials. ZrO_2 [$Zr(OC_4H_9)_4$, Aldrich], TiO_2 [$Ti(OC_4H_9)_4$, Kishida], trimethylphosphate [$PO(OCH_3)_3$, Kishida], and *N*,*N*-dimethylformamide (Kishida, 99%) were used without further purification. Solvents (TEOS, SiO_2, and ethanol) and reagents of analytical grade were commercial products and were used as received. Water purified with a Milli-Q system from Millipore (AQUARIUS/GS-20R) was used for all experiments.

2.2. Synthesis of Glass Membranes. Glass membranes were prepared via a sol−gel process according to a procedure similar to what can be found in our previous reports.[17] The electrodes were prepared via a conventional method with Nafion, polytetraflouroethylene (PTFE), Pt/C powder (0.1 mg/cm^2), and solvents (deionized water and ethanol). The thickness of the glass membranes ranged between 0.3 and 1 mm, and the

* Corresponding authors. Tel.: +81 52 735 5285; fax: +81 52 735 5285; e-mail: (T.U.) ptuma2002@yahoo.co.in and (M.N.) nogami@mse.nitech.ac.jp.

10.1021/jp075015z CCC: $37.00
Published on Web 10/09/2007

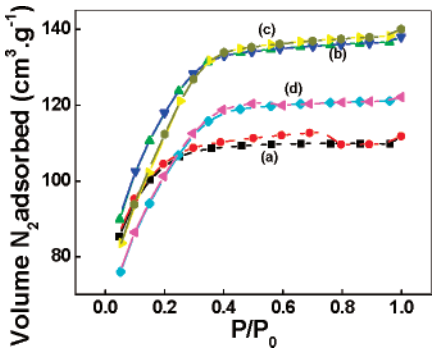

Figure 1. N_2 adsorption−desorption isotherms of $TiO_2/ZrO_2-P_2O_5-SiO_2$ glass composite membranes: (a) 1:2:5:92 (mol %) (b) 2:3:5:90 (mol %), (c) 3:4:5:88 (mol %), and (d) 4:5:5:86 (mol %). Samples were degassed at 250 °C for 5 h before measurement.

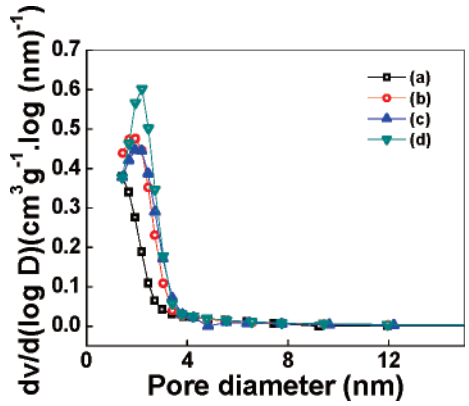

Figure 2. Pore properties of $TiO_2/ZrO_2-P_2O_5-SiO_2$ glass composite membranes: (a) 1:2:5:92 (mol %) (b) 2:3:5:90 (mol %), (c) 3:4:5:88 (mol %), and (d) 4:5:5:86 (mol %) determined with the BET method.

thickness of the electrode was 0.21 mm. The preparation of the Pt/C electrode has been described in detail elsewhere.[18]

2.3. Characterization of the Glass Composite Membranes. The Brunauer−Emmett−Teller (BET) specific surface areas of the mixed composite membranes were determined from N_2 adsorption−desorption isotherms at the temperature for liquid nitrogen. Prior to the measurements, the samples were degassed at 250 °C for 5 h. The pore size distributions were analyzed with a Quantochrome-NOVA-1000 nitrogen gas sorption analyzer. Fourier transform infrared (FTIR) spectra of powders of the glasses were obtained in the 4000−600 cm^{-1} range using a JASCO FTIR-460 spectrometer. The thermal stability was evaluated with a Thermoplus-2 (TG-8120, RIGAKU) analyzer. The thermogravimetric and differential thermal analyses were performed under nitrogen atmosphere at a heating rate of 10 °C/min on 10 mg of the glass powder samples. The studied temperature range was 30−800 °C. The ac proton conductivity measurements were conducted on a Solartron 1260 frequency analyzer in the frequency range of 0.1 Hz to 1 MHz. The amplitude of the ac voltage was 10 mV, and the measurements were carried out in the temperature range of 30−80 °C with a variation in humidity between 30 and 80%. The initial value of the electrical resistance was used to calculate the specific conductivity. The hydrogen permeability of glass composite membranes (1 mm thick) was measured using an in forced convection drying oven (DO-600FA) in the temperature range of 30−110 °C.

3. Results and Discussion

3.1. Textural Analysis. Figure 1 shows N_2 adsorption−desorption of $TiO_2/ZrO_2-P_2O_5-SiO_2$ glass composite membranes with varying compositions. The figure displays type IV adsorption isotherms with a well-defined step around $P/P_0 = 0.99$, characteristic of capillary condensation within uniform pores. Sol−gel-derived glasses are porous, the pore surfaces of which are terminated with hydroxyl bonds and the adsorbed water in a humid atmosphere. The glass samples were heated at 600 °C, thus leading to the removal of water and formamide and subsequently to a polycondensation between surface and SiOH groups. When heated, the gels transform into glass according to dehydration and polycondensation by sintering. The water in the gel was divided into four types: (i) physically and (ii) chemically adsorbed water in pores, (iii) surface OH groups bonded with Si^{4+} ions, and (iv) OH groups surrounded with a silica glass network structure. We have discovered that proton conduction is promoted by the dissociation of protons from the hydroxyl bonds on the pore surfaces and a hopping of the protons between hydroxyl groups and water molecules.[19,20] The conduction of protons in the glass membrane is mainly due to the hopping of protons through the hydrogen-bonding water and hydroxyl groups in the network structure, leading to the protons being transported on the surfaces of the pore channels. The contribution of surface and bulk transport mechanisms, respectively, decreases or increases with an increase in the pore size of the membrane channels. These pore characteristics, such as the pore size and the functional groups of the glass membranes, are responsible for the increase in conductivity.[1,2]

The pore size and surface area properties of the phosphosilica sol−gel matrix incorporated with TiO_2/ZrO_2 are shown in Figure 2. The isotherms indicated mesopores with pore sizes below 2.5 nm for all glass membranes. The height of the plateau increased for an increasing concentration of TiO_2/ZrO_2 in the glass composition (Figure 1a−c), except for the sample with a TiO_2/ZrO_2 concentration of 4/5 mol %, where was found to decrease the plateau height (Figure 1d). Moreover, the sharpness of the knee region also decreased. The variation of the specific surface areas for all glass membranes is given in Figure 2. Here, one can observe a decrease in the specific surface area and pore volume and an increase in the pore size for all glass samples. The average pore size was about 2.2 nm; the pore volume was in the range of 0.217−0.173 cm^3/g, and the specific area displayed values of 396−315 m^2/g. While the pore volume and the surface area both decreased continually with the time of the heat treatment, the shape of the pore size distribution remained basically the unchanged. Under degassed conditions (250 °C), the glass samples resembled mesopores, and the adsorptions were shifted to a higher relative pressure, denoting large pores. This represents a significant improvement for potential applications of such materials.

3.2. FTIR Analysis. FTIR has proven to be a good method for following the hydrolysis and condensation reactions in sol−gel processes, and FTIR spectra of glass composite membranes with varying compositions can be seen in Figure 3.[21,22] Typical IR features of anhydrous P_2O_5 glass were the P═O band at 1378 cm^{-1} and the asymmetric and symmetric P−O−P stretching bands at 930 and 787 cm^{-1}, respectively. No band due to P═OH was observed, and νP_2O_5 was IR inactive in the 1000−1300 cm^{-1} region. A new band at 1300 cm^{-1} appeared and was found to develop into a well-defined band with increasing TiO_2 content up to 4 mol % and a ZrO_2 content of 5 mol % (Figure 3d). The characteristic band of the out-of-chain PO_2 units at 1265 cm^{-1} merged with the 1306 cm^{-1} band and grew in intensity to form a single band in the spectra. The frequency of the symmetric P−O−P band increased from 925 to 941 cm^{-1} by increasing the concentration of TiO_2/ZrO_2 in the glass

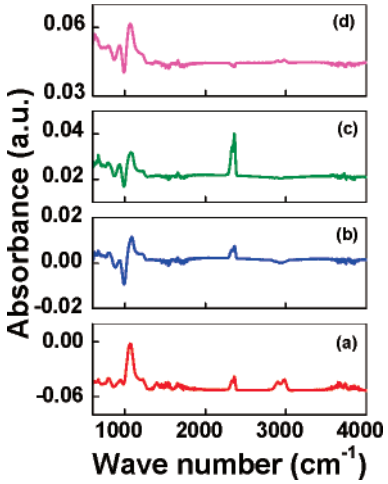

Figure 3. FTIR spectra of $TiO_2/ZrO_2-P_2O_5-SiO_2$ glass composite membranes: (a) 1:2:5:92 (mol %) (b) 2:3:5:90 (mol %), (c) 3:4:5:88 (mol %), and (d) 4:5:5:86 (mol %). Spectra were recorded in absorbance mode on glass powders in the wavenumber range of 4000−600 cm^{-1}.

composite membranes. The IR spectra also showed that both OH groups and H_2O molecules were present in the glasses and that most of the water related species were strongly H-bonded. The absence of measurable conductivity in hydrous silica glass was a fact only in the presence of nonbridging oxygens. The wavenumbers for the IR peaks approached constant values. The dispersion of Ti in a SiO_2 matrix is usually associated[15] with the ratio of infrared vibrations due to a (Zr) Ti−O−Si band at 930−960 cm^{-1} and to that of Si−O−Si at ca. 1200 cm^{-1}.

The intensity of the absorption band for Si−O−Ti bonding can be seen as an indication of the degree of inclusion of titanium ions in the silica structure. To confirm that the absorption band observed at 950 cm^{-1} for the gel-derived TiO_2-SiO_2 particles was not caused by the existence of Si−OH bonds but rather of Si−O−Ti bonding, gel-derived SiO_2 particles were prepared using the same conditions as those for TiO_2-SiO_2 particles and were subsequently analyzed by FTIR. The band at ca. 950 cm^{-1} was assigned to Si−O−Ti stretching.[23,24] This band has been ascribed to a vibration involving SiO_4 tetrahedra bonded to a 4-fold coordinated titanium atom and indicates a good mixing of Ti and Si at the atomic level.[25] This feature has also been assigned to the stretching vibration of silanol groups in pure silica.[26] In this way, the band located around 950 cm^{-1}, in the present work, could be a superimposed band with coupled vibrational modes of Si−O^- stretching and Si−O−Ti linkages. The dispersion of Ti in a SiO_2 matrix is usually[23] associated with the ratio of infrared vibrations between the Ti−O−Si band at 930−960 cm^{-1} and that due to Si−O−Si at ca. 1200 cm^{-1}.

IR reflection spectra of glass have been found to vary with the phase separation in the glass.[27,28] In particular, a shift of the IR reflection peak of the silica structural band was found to be a sensitive means of detecting phase separation in glasses.[29] There are two important infrared absorption bands due to the O−H stretching vibration in oxide glasses. One set of vibrations occurs at around 3000 cm^{-1} (band 1), and a second set occurs around 2900 cm^{-1} (band 2). The protons involved in the band 1 vibrations are not hydrogen bonded.[30] We have found that the hydrogen-bonded protons are much more mobile than their nonhydrogen-bonding counterparts.[31] In glass containing no molecular water, the electrical charge carriers have been proven to be protons.[32] The water content in the glasses was determined by infrared spectroscopy.[33] For other water related features observed in the IR spectrum, tentative assignments in the literature relate the 3608 cm^{-1} shoulder to OH stretching of

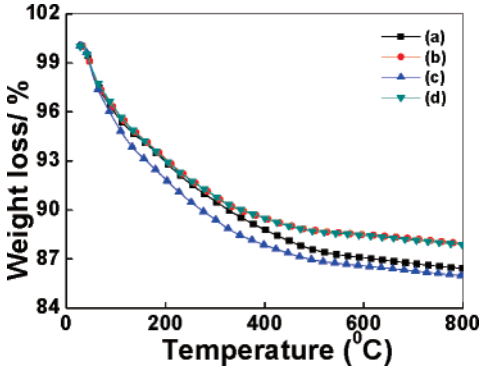

Figure 4. TGA plots of $TiO_2/ZrO_2-P_2O_5-SiO_2$ glass composite membranes: (a) 1:2:5:92 (mol %) (b) 2:3:5:90 (mol %), (c) 3:4:5:88 (mol %), and (d) 4:5:5:86 (mol %). All TGA curves were recorded on glass powders between room temperature and 800 °C, under a nitrogen atmosphere and at a heating rate of 10 °C/min.

silanol, which is hydrogen bonded to an unspecified species,[32] the ∼3400 cm^{-1} band to molecular water,[34] and the 2910 cm^{-1} band to OH stretching of the hydroxyl, which is hydrogen bonded to the nonbridging oxygen in the glass.[35]

Two main absorbance peaks appeared in the measured IR range with wavenumbers of 3670 and 3425 cm^{-1}, respectively. The peak at 3670 cm^{-1} was attributed to the hydroxyl (−OH) and the peak at 3425 cm^{-1} to molecular water (H_2O) by a detailed peak separation method.[36] A peak near 3600 cm^{-1} has been attributed to hydrogen-bonded hydroxyls.[37] In addition, free molecular water is known to give rise to an IR peak at 3225 cm^{-1}. Measuring this peak makes it possible to obtain the concentration of the free molecular water. The absorption band near 880−917 cm^{-1} was assigned to the asymmetric stretching mode of the P−O−P linkages, while the two modes around 725−785 cm^{-1} were attributed to the symmetric stretching of the P−O−P groups. The bands at 1050 cm^{-1} were assigned to stretching and deformation modes of the PO_4^{3-} groups.[38] Single phosphorus centers in phosphosilicate glass designated as O═P(O−−Si)$_3$ were simulated by O═P−(−O−EnDashSiH_3)$_3$ clusters containing a single O═PO_3 tetrahedron bonded with three Si atoms, of which the dangling bonds were saturated by H atoms. Recently, new technologies have been implemented to establish new and improved limits in size, specific surface, and porosity for raw materials. The chemical reactions that occur during the aging process change the morphology and structure in the silica network, giving rise to strengthening and stiffening. These structural changes have an important effect on the subsequent drying step.

3.3. Thermal Analysis. TG and DTA curves of the glass composite membranes with varying compositions are shown in Figures 4 and 5, respectively. The thermal stability is an important property for proton conducting glass membranes to be used in fuel cells. The first evidence of weight loss that occurred just below 100 °C was most probably due to the evaporation of residual water present in the membranes. It can be seen that all membranes (Figure 4a−d) displayed a thermal stability at about 100 °C with a small weight loss of around 5.1%. This was mainly due to the vaporization of physisorbed water within pores in the network structure of the glass membranes. When the temperature was raised to 300 °C, the weight loss of all glass membranes was below 10.8% and was accompanied by an exothermic peak at 300 °C in the DTA curve, which can be attributed to the loss of absorbed water and isolated phosphoric acid. The weight loss of about 8.9% at a temperature of 250 °C was attributed to the desorption of chemisorbed water and hydroxyl groups via hydrogen bonding

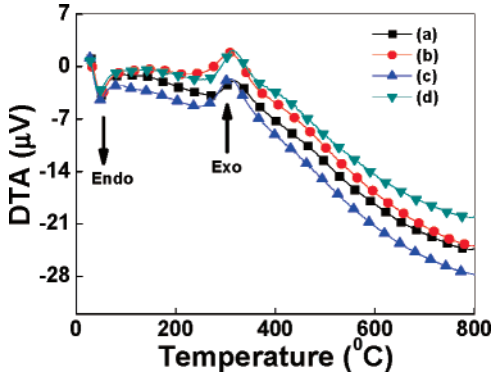

Figure 5. DTA plots of $TiO_2/ZrO_2-P_2O_5-SiO_2$ glass composite membranes: (a) 1:2:5:92 (mol %) (b) 2:3:5:90 (mol %), (c) 3:4:5:88 (mol %), and (d) 4:5:5:86 (mol %). All DTA curves were recorded on powder samples from room temperature to 800 °C under a nitrogen atmosphere and at a heating rate of 10 °C/min.

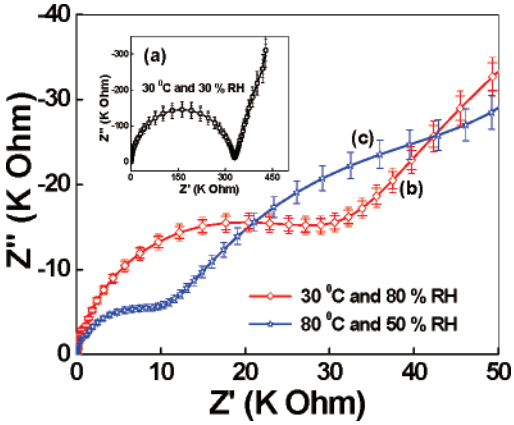

Figure 6. AC impedance plots of $TiO_2/ZrO_2-P_2O_5-SiO_2$ (4:5:5:86 mol %) glass composite membrane at varying temperatures and RH. Inside impedance curve shows that the conductivity was measured at 30 °C and 30% RH. Impedance measurements were carried out in the temperature region of 30−80 °C with a constant RH of 30−80%.

to the oxygen atoms of SiOH and POH in the glass membrane. A final weight loss of about 13% was observed at around 400 °C and was ascribed to the removal of the adsorbed water and hydroxyl groups via strong hydrogen bonding to the oxygen atom of POH in the network structure of the glass membrane. As compared with SiOH, the proton in the POH group is strongly hydrogen bonded with the water molecules, resulting in a high temperature being necessary to remove the water from POH. A weight loss of about 5.1−13% in the range from room temperature to 400 °C was observed for all samples in TGA (Figure 4a−d).

The DTA curves also displayed a large endothermic peak at about 43 °C and an exothermic peak at 300 °C for all samples (Figure 5a−d). DTA confirmed that glasses had noncrystalline phases. The endotherm corresponded to the loss of water molecules and the residual inorganic groups from the porous gel samples. The exothermic peak appeared at 300 °C on the DTA curve, indicating the formation of an interfacial compound observed in the glass composites $TiO_2/ZrO_2-P_2O_5-SiO_2$. This exothermic peak indicated that the thermal stability of these glass materials was quite sufficient for low-temperature H_2/O_2 fuel cell application. Depending on the bulk composition and water content, such glasses have a high thermal stability. Moreover, with increasing water content, the decomposition temperature of the glass membrane slightly increased. This was a result of water molecules, with highly reactive hydroxyl end groups at the surface of the molecules, being able to act as cross-link points. In this way, the degree of cross-linking of the membranes was increased, and ultimately, their thermal stability could be enhanced.

3.4. Proton Conductivity. Figure 6 presents Cole−Cole plots displaying the complex impedance Z (i.e., the real (Z') vs the imaginary (Z'') parts) at varying temperatures and humidities for the $TiO_2/ZrO_2-P_2O_5-SiO_2$ (4:5−:5:86 mol %) glass composite membrane. As depicted in Figure 6a, a semicircular arc of a higher radius is found for the lowest RH of 30%. As the RH increased to 50%, the radius diminished, thus giving rise to a semicircle along with an incomplete arc. When increasing the RH, the diameter of the semicircle at a higher frequency became smaller. Plots of Z' versus Z'' in Figure 6b,c indicate the same characteristic features with the basic difference being that the separation into two semicircles for the samples depended on the relative humidity between 30 and 80%. The proton conductivity varied from 2.3×10^{-3} S cm^{-1} at 30 °C with 30% RH to 4.2×10^{-3} S cm^{-1} at 30 °C with 80% RH. The conductivity (5.8×10^{-3} S cm^{-1}) was found to increase with an increasing temperature at 80 °C with 50% RH. These values have a similar order of magnitude but were higher than values previously reported for phosphosilicate glasses doped with TiO_2 and ZrO_2.[17,18] The amount of the adsorbed water in the gels must increase with an increase in relative humidity, so that continuous paths suitable for fast proton conduction are formed in the gels due to the adsorption of water. Furthermore, glasses with high concentrations of OH groups are potential proton conductors. Water is dissolved in silicate glasses in the form of at least two different water species: −OH groups and H_2O molecules.[39,40] The main characteristic change is the protonic conduction due to the sorption of water molecules, which primarily depends on the porosity of the materials.

An impedance curve, at low frequencies, which becomes more pronounced with increasing temperature, originates from the thermally activated hopping process of mobile ions. In this high-frequency range, the conductivity strongly increases with frequency (dispersive range), which can be attributed to a contribution of forward−backward hops of the ions.[41] The zirconium phosphate glasses had a high concentration of hydrogen-bonded protons from hydroxyl groups (−OH) and molecular water. The conductivity data were obtained for glasses containing small amounts of water, and the result suggests that the mobility of the protons in the glasses increased with decreasing O−H-bonding strength. Water in glass has disproportionately large effects on various properties of oxide glasses, such as chemical durability and mechanical strength. The conductivity of glass composites improved with an increase in the molar ratio of TiO_2/ZrO_2. Accordingly, in TiO_2/ZrO_2-doped glass membranes, ZrO_2 should be responsible for the high proton conductivity and TiO_2 serve as a supporting matrix. This subject will be studied further in a future investigation.

3.5. Hydrogen Permeability. The hydrogen permeability based on the glass membranes (thickness = 1.1 mm) was evaluated in the temperature range of 30−110 °C and is shown in Figure 7. The permeability was found to decrease as a function of temperature, and a value of 3.83×10^{-12} mol/cm s Pa was observed at 110 °C. This indicates that the hydrogen permeation kinetics was controlled by the transport of charge carriers in the glass composite membrane. As a comparison, the permeability of Nafion 117 was 3.01×10^{-13} mol/cm s Pa at 30 °C, as obtained in our lab. Furthermore, the hydrogen permeability of $P_2O_5-SiO_2$, $TiO_2-P_2O_5-SiO_2$, and $ZrO_2-P_2O_5-SiO_2$ glass electrolytes (thickness = 0.7−0.8 mm) were determined to be 10^{-10} to 10^{-12} cm^2/s under similar conditions.

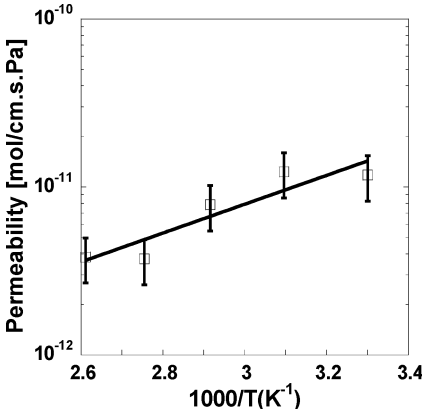

Figure 7. Hydrogen permeation rate as a function of inverse temperature for the $TiO_2/ZrO_2-P_2O_5-SiO_2$ (4:5:5:86 mol %) glass composite membranes. The permeability measurement was performed under hydrogen feed in the temperature range of 30−110 °C.

The mixed $TiO_2/ZrO_2-P_2O_5-SiO_2$ glass membrane also displayed a permeability on the order of 10^{-10} to 10^{-12} mol/cm s Pa. This value was 2 orders of magnitude higher than the corresponding value for the Nafion membrane. The permeability coefficient of any gas through a membrane is directly related to the size and thickness of the membrane. Improvements in electronic (and H_2) transport rates require higher electron/hole diffusivities or more reducible membrane materials, which increase electron concentrations for a given chemical environment. Simulation results illustrate the nature and underlying mechanism for the observed effects of the chemical environment in each side of the membrane on H_2 permeation rates and how such effects depend on membrane properties, such as reducibility and charge carrier mobility. Also, the subject of hydration permeation in glass membranes requires a deeper investigation and will be the objective of a future study.

4. Conclusion

Porous glass composite membranes displayed maximum conductivities of 5.8×10^{-3} S cm^{-1} at 80 °C and 50% RH. To confirm that the absorption band observed at 950 cm^{-1} for gel-derived TiO_2-SiO_2 particles was not caused by the existence of Si−OH bonds but rather by Si−O−Ti bonding, gel-derived SiO_2 particles were prepared under equivalent conditions as those for TiO_2-SiO_2 particles and were analyzed by FTIR. TG/DTA results displayed that the obtained glass membranes were thermally stable and that the glasses had not contained any crystalline phases. From the textural properties, an average pore size of 2.2 nm was recorded by the BET method. All these characteristics render the composites very attractive for electrochemical devices, in particular, for low-temperature fuel cells. A hydrogen permeability of 3.83×10^{-12} mol/cm s Pa was recorded at 110 °C for a mixed inorganic glass membrane.

Acknowledgment. The authors acknowledge financial support from the Japan Society for the Promotion of Science (JSPS) fellowship program.

References and Notes

(1) Kreuer, K. D. *Chem. Mater.* **1996**, *8*, 610.
(2) Glasser, L. *Chem. Rev.* **1975**, *75*, 21.
(3) Rubia, F. S. L.; Wander, L. V. *Appl. Phys. Lett.* **2002**, *5*, 497.
(4) Lee, D. W.; Ihm, S. K.; Lee, K. H. *Euromembrane* **2006**, *199*, 363.
(5) Ozkan, U. S.; Watson, R. B. *Catal. Today* **2005**, *100*, 101.
(6) Neumann, R.; Chava, M.; Levin, M. *J. Chem. Soc., Chem. Commun.* **1993**, *8*, 1685.
(7) Notari, B. *Catal. Today* **1993**, *18*, 163.
(8) Millar, J. B.; Jonhston, S. T.; Ko, E. I. *J. Catal.* **1994**, *150*, 311.
(9) Scharttka, J.; Shchukin, D.; Jia, J.; Antonietti, M.; Caruso, R. *Chem. Mater.* **2002**, *14*, 5103.
(10) Dutoit, D. C. M, Schneider, M.; Baiker, A. *J. Catal.* **1995**, *153*, 165.
(11) Hay, J. N.; Raval, H. M. *J. Mater. Chem.* **1998**, *8*, 1233.
(12) Tarafdar, A.; Panda, A. B.; Pramanik, P. *Microporous Mesoporous Mater.* **2005**, *84*, 223.
(13) Anderson, J. A.; Fergusson, C. A. *J. Mater. Sci. Lett.* **1999**, *18*, 1075.
(14) Zhu, D.; Kosugi, T. *J. Non-Cryst. Solids* **1996**, *202*, 88.
(15) Dhar, H. P. *J. Electroanal. Chem.* **1993**, *357*, 237.
(16) Appleby, A. J. *Philos. Trans. R. Soc. London, Ser. A* **1996**, *354*, 681.
(17) Uma, T.; Nogami, M. *J. Electrochem. Soc.* **2007**, *154*, 845.
(18) Uma, T.; Nogami, M. *J. New Mater. Electrochem. Syst.* **2007**, *10*, 75.
(19) Nogami, M.; Abe, Y. *Phys. Rev. B: Condens. Matter Mater. Phys.* **1997**, *55*, 12108.
(20) Nogami, M.; Nagao, R.; Wong, C.; Kasuga, T.; Hayakawa, T. *J. Phys. Chem. B* **1999**, *103*, 9468.
(21) Matos, M. C.; Ikharco, L. M.; Almeida, R. M. *J. Non-Cryst. Solids* **1992**, *147−148*, 232.
(22) Ying, J.; Bensigar, J. B.; Navrotsky, A. *J. Am. Ceram. Soc.* **1993**, *76*, 2561.
(23) Dutoit, D. C. M.; Schneider, M.; Baiker, A. *J. Catal.* **1995**, *153*, 165.
(24) Salvado, I. M. M.; Navarro, J. M. F. *J. Non-Cryst. Solids* **1992**, *147−148*, 256.
(25) Beghi, M.; Chiurlo, P.; Costa, L.; Palladino, M.; Pirini, M. F. *J. Non-Cryst. Solids* **1992**, *145*, 175.
(26) Aizawa, M.; Nosaka, Y.; Fuji, N. *J. Non-Cryst. Solids* **1994**, *168*, 49.
(27) Katao, Y.; Yamazaki, H.; Tomozawa, M. *J. Am. Ceram. Soc.* **2001**, *84*, 2111.
(28) Takashima, H.; Kato, E.; Saito, H. *Yogyo-Kyokai-Shi* **1973**, *81*, 238.
(29) Takashima, H.; Kato, E.; Saito, H. *Yogyo-Kyokai-Shi* **1974**, *82*, 47.
(30) Scholze, H. *Glastech Ber.* **1959**, *32*, 81, 142, 314.
(31) Abe, Y.; Hosono, H.; Ohta, Y.; Hench, L. L. *Phys. Rev. B: Condens. Matter Mater. Phys.* **1988**, *38*, 10166.
(32) Hosono, H.; Kamae, T.; Abe, Y. *J. Am. Ceram. Soc.* **1989**, *72*, 294.
(33) Wakabayashio, H.; Tomozawa, M. *J. Am. Ceram. Soc.* **1989**, *72*, 1850.
(34) Wakabayashio, H. *Trans. Mater. Res. Soc. Jpn.* **1992**, *8*, 426.
(35) McMillan, P. F.; Remmele, R. L. *Am. Mineral.* **1986**, *71*, 772.
(36) Davis, K. M.; Tomozawa, M. *J. Non-Cryst. Solids* **1996**, *201*, 76.
(37) Walrafen, G. E.; Samanta, S. R. *J. Chem. Phys.* **1978**, *68*, 483.
(38) Salim, M. A.; Khattak, G. D.; Hussain, M. S. *J. Non-Cryst. Solids* **1995**, *185*, 101.
(39) Szirtes, L.; Szirtes, L. *Magy. Kem. Foly.* **1967**, *74*, 258.
(40) Bartholomew, R. F.; Butler, B. L.; Hoover, H. L.; Wu, C. K. *J. Am. Ceram. Soc.* **1980**, *68*, 481.
(41) Behrens, H.; Romano, C.; Nowak, M.; Holts, F.; Dingwell, D. B. *Chem. Geol.* **1996**, *128*, 41.